



## Frequency-dependent microstructural characteristics and corrosion behavior of oxide coatings on Ti-6Al-4V alloy fabricated by plasma electrolytic oxidation

Elham Nikoomanzari<sup>1</sup>, Arash Fattah-alhosseini<sup>1,\*</sup>

<sup>1</sup>Department of Materials Engineering, Bu-Ali Sina University, Hamedan, 65178-38695, Iran.

Received: 19 Oct 2023; Accepted: 14 Dec 2023

\*Corresponding author email: [a.fattah@basu.ac.ir](mailto:a.fattah@basu.ac.ir)

### ABSTRACT

This study investigated the influence of three different frequencies (100, 1000, and 2000 Hz) during the PEO process on the characteristics of ceramic coatings fabricated on Ti-6Al-4V alloys in the presence of 12 g/L Na<sub>3</sub>PO<sub>4</sub>·12H<sub>2</sub>O and 3 g/L ZrO<sub>2</sub> nanoparticles. The microstructure, surface roughness, wettability, chemical composition, and corrosion performance of the coatings were thoroughly examined to assess their performance. The microstructural results revealed that increasing frequencies led to a reduction in the porosity size, as well as a decrease in coating thickness, wettability, and surface roughness. Additionally, the corrosion performance of the coatings was evaluated in Hank's solution using electrochemical impedance spectroscopy (EIS) and potentiodynamic polarization (PDP) methods. As the frequency rose from 100 to 2000 Hz, the corrosion current density dropped significantly from 47.35 to 13.75 nA/cm<sup>2</sup> and the corrosion potential increased from 218 to 684 mV versus Ag/AgCl electrode. These findings indicated that the coating produced at a frequency of 2000 Hz exhibited the lowest corrosion density, thereby demonstrating superior corrosion resistance compared to the coatings produced at lower frequencies. The corrosion resistance of the optimum coating (coating formed at a frequency of 2000 Hz) was found to be approximately 0.8 times higher compared to the uncoated metal.

Keywords: ZrO<sub>2</sub> nanoparticles; Ti-6Al-4V; Plasma electrolytic oxidation (PEO); Frequency; Corrosion behavior.

### 1. Introduction

Titanium and its alloys have excellent engineering properties that make them suitable for various industries, such as low corrosion susceptibility, high strength-to-weight ratio, and high melting point [1]. Consequently, the demand for titanium alloys in industries such as biomedical, marine, and aerospace is rapidly growing [2,3]. However, titanium and its alloys have limited applications due to their high friction coefficient and low wear resistance. In recent years, plasma electrolytic oxidation (PEO)

has been proven to be a highly valuable technique for the formation of protective oxide coatings with thickness varying between 5 and 200 μm [4,5]. Under oxidizing conditions and voltages exceeding the breakdown voltages of the primary oxide films (approximately 150–800 V), PEO creates ceramic coatings on Ti alloys that are biocompatible and resistant to corrosion [6]. High temperatures and high pressure within discharge channels, caused by electrical discharges and gas evolution, lead to the growth of an oxide coating on the anode surface

[7]. The PEO process involves the dissolution of the substrate surface, and ionization of the electrolyte, followed by a reaction between the negatively charged ions and the substrate. The final coating exhibits a dual-layer structure, with the outer layer being appropriate for biological uses, and the inner layer providing enhanced resistance to corrosion [8,9]. The size, intensity, and lifetime of micro-discharges are significantly influenced by the electrolyte concentration, processing time, and type, as well as electrical parameters, making them the most crucial factors to consider [10,11].

Extensive research has been conducted to optimize the parameters that influence the PEO process, aiming to enhance the coating's properties for diverse applications [12]. A notable endeavor is the modification of electrolyte composition through the addition of nano or micro-particle, which results in the creation of composite coatings with desirable characteristics [13]. Inert incorporation is the term used when particles are added to a material without causing any reaction or new phase formation. In such cases, the shape and size of the particles remain unchanged, making them easily identifiable in the layer. However, there may be some superficial reactions occurring in the interfacial region between the coating matrix and the particles. Nonetheless, the particles themselves undergo no significant changes. High-energy discharges in the PEO processing can cause the particles to melt and interact with other elements in the electrolyte and matrix. This is known as reactive or partly reactive incorporation. This intricate process is influenced by several factors, including the substrate material, particle size, concentration, melting point, and zeta potential. Additionally, the base electrolyte composition and the discharge energy are important factors that affect the degree of the reaction [14,15]. In our previous study [16], we conducted an investigation on the impact of zirconia nanoparticle concentration on the chemical composition, corrosion behavior, and antibacterial properties. The XRD analysis revealed that the presence of the zirconia nanoparticles resulted in the formation of Zr-TiO<sub>4</sub> (zirconium titanate) phases. Additionally, the corrosion test results demonstrated that the coating

containing of 3 g/L zirconia nanoparticles exhibited the most favorable corrosion behavior. Beyond this concentration of nanoparticles, the surface discontinuity increased and the corrosion resistance decreased.

The electrical parameters, such as voltage [17] (or current density [18]), duty ratio [19], and frequency [20] are very important in the PEO process. They affect both how the coating grows and what its composition and structure are. As a result, extensive research has been carried out to explore the impacts of aforementioned parameters on the characteristics of PEO coatings. It is suggested that as the frequency increases, the duration of one cycle decreases, leading to more interruptions per second and less energy imparted by each cycle, which in turn produces weaker electrical sparks [21]. So far, no study has been conducted on investigating the influence of frequency on corrosion performance of PEO-derived coatings fabricated on titanium-based alloys in an electrolyte containing zirconia nanoparticles. So, this study aimed to examine the impact of frequency on the characteristics of ZrO<sub>2</sub>-incorporated PEO coatings formed on Ti-6Al-4V using a phosphate-based electrolyte. The objective was to determine an optimal range of frequency that would improve the surface characteristics and electrochemical properties of the PEO-based surface coating, which were assessed by potentiodynamic polarization and electrochemical impedance spectroscopy.

**2. Experimental Procedure**

The substrate for the PEO process in this investigation was the Ti-6Al-4V, whose chemical composition showed in Table 1. In the initial stage of sample preparation, the samples were polished using grinding papers ranging from 60 to 800. Subsequently, the samples were cleansed with distilled water and dried using a blast of cold air. A DC pulsed power supply (PM 700/7 PRC (IPS)) with a maximum voltage of 700 V was utilized to carry out the PEO process. Following this, the cylindrical stainless steel container equipped with a cooling system and the prepared samples were connected to the negative (cathode) and positive (anode) ter-

Table 1- Chemical composition of Ti-6Al-4V alloy

Element	Al	V	O	Fe	C	N	Ti
wt.%	5.80	4.12	0.06	0.05	0.01	0.009	Surplus

minerals of the device, respectively. The specimens were submerged in a solution with deionized water,  $\text{Na}_3\text{PO}_4 \cdot 12\text{H}_2\text{O}$  at a concentration of 12 g/L, and  $\text{ZrO}_2$  nanoparticles at a concentration of 3 g/L. The zirconia nanoparticles, with an average size of approximately 40 nm, were obtained from a US research company. It is worth noting that a previous study conducted by our research group determined that the optimal concentration of  $\text{ZrO}_2$  nanoparticles and current density were 3 g/L and 2 A/dm<sup>2</sup>, respectively. Due to the pivotal role of frequency in the PEO process, the coatings were prepared using various frequencies including 100, 1000, and 2000 Hz, labeled as F100, F1000, and F2000, respectively. All experiments were carried out over a duration of 10 minutes.

In order to ascertain the phase composition of coatings, X-ray diffraction analysis were performed utilizing Cu K $\alpha$  ( $\lambda = 1.5406 \text{ \AA}$ ) radiation. The XRD analysis was conducted at diffraction angles range of 10° to 80°, with a step size of 0.10°. The XRD patterns were assessed using the PANalytical X'Pert High Score software, which utilizes the International centre for diffraction data (ICDD) database. To examine both the cross-section and surface microstructure of the coatings, a scanning electron microscope (JEOL JSM-840A) was used. Prior to the cross-sectional analysis, all coatings underwent polishing using grinding papers ranging from 60 to 3000. The porosity size and thickness of coatings were calculated using MIP software. A digital photography device attached with an optical microscope was used to assess the wettability angle of the coatings using the sessile drop method using Hank's solution. The average value of three

measurements for each sample was recorded. The surface roughness of the specimens was evaluated using the RT2200 model surface roughness tester. Experiments were conducted at three distinct zones, and then the mean value of was stated. To investigate the corrosion performance of both untreated and the PEO coatings, electrochemical techniques including potentiodynamic polarization (PDP) and electrochemical impedance spectroscopy (EIS) were conducted in Hank's electrolyte [16]. The corrosion assessments were conducted using a  $\mu$ Autolab Type III/FRA2 instrument, which utilizes a three-electrode compartment. This includes a saturated Ag/AgCl electrode serving as a reference electrode, a platinum rod acting as a counter electrode, and a specimen with an active area of 0.7 cm<sup>2</sup> functioning as the working electrode. Prior to conducting the experiments, the working electrodes were submerged in the electrolyte for a duration of 7200 seconds in order to achieve a stable state. The PDP measurements were carried out from -250 mV relative to the open circuit potential, at a scanning rate of 1 mV/s. The EIS tests were conducted over a frequency range from 100 kHz to 10 mHz, with a wavelength range of  $\pm 10$  mV. To confirm the precision of the results, each experiment was repeated at least twice. NOVA 2.1 software was used to analyze the corrosion test results.

### 3. Results and Discussion

#### 3.1. Microstructure, roughness and wettability of PEO coatings

The morphologies of the surface and cross-section of coatings with various frequencies are depicted in Fig. 1. It is evident that all the surfaces (Fig. 1(a-c))

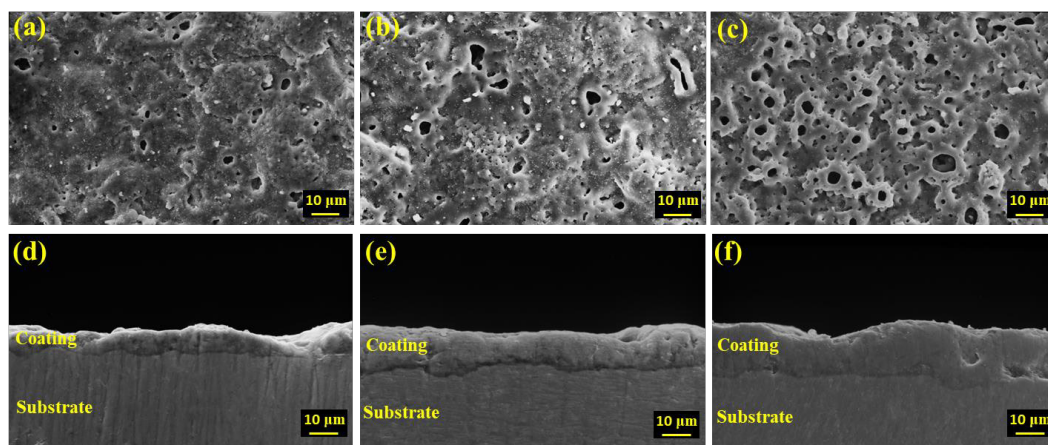


Fig. 1- SEM micrographs of cross-section and surface of coatings obtained from plasma electrolytic oxidation procedures: (a, d) F2000, (b, e) F1000, (c, f) F100.

are characterized by the presence of porosities and micro-cracks. When the dielectric breakdown potential is attained, the negative ions in the electrolytes are drawn towards the substrate and infiltrate the channels where discharges take place. Under conditions of high pressure and temperature, the substrate undergoes oxidation and melting, subsequently entering the channels. Subsequently, the substances that have undergone oxidation emerge from the channels and accumulate as a deposit on the surface [22]. The gases, which are emitted via the channels where discharges occur, lead to the formation of porosities on the coating surface [23]. On the other hand, the presence of micro-cracks resulted from the release of thermal stress induced by the interaction between the molten material and the relatively cold electrolyte [24]. The pore size in F100, F1000 and F2000 samples were about 5.7, 3.2 and 1.6  $\mu\text{m}$ , respectively. Indeed, as the frequency escalated from 100 to 2000 Hz, there was a relative reduction in the anode process, leading to the occurrence of more dispersed and smaller discharging sparks [25]. It should also be noted that the porosity percentage of F2000, F1000 and F100 were measured to be 1.11%, 1.31%, and 9.52%, respectively. Fig. 1 (d-f) displays the cross-sections of coatings prepared at various frequencies. It is apparent that there was a satisfactory bond between the substrate and all the coatings. At a frequency of 2000 Hz, a coating with an average thickness of 7.1  $\mu\text{m}$  was achieved. Moreover, the average thickness of coatings formed at frequencies of 1000 Hz and 100 Hz was about 10.7  $\mu\text{m}$  and 14.6  $\mu\text{m}$ , respectively. An increase in thickness of coating at lower frequency can be attributed to the longer anode process. In fact, as the frequency decreased, the duration of the anode process increased, resulting a higher energy output per pulse, which ultimately facilitated the increased growth rate [26,27]. The FESEM images from the surface of the F2000 sample are given in Fig. 2. The visible bright agglomerated particles were observed on the surface of coating (Fig. 2a) and the  $\text{ZrO}_2$  nanoparticles in the range of 19 to 45  $\mu\text{m}$  were seen at higher magnification (Fig. 2b). Fig. 3 illustrates the correlation between surface roughness and wettability. It is apparent that the  $R_a$  values of the coatings increased compared to the substrate. Surfaces are deemed smooth if their roughness values are below 1  $\mu\text{m}$ , while those with roughness values exceeding 1  $\mu\text{m}$  are considered rough [28]. Consequently, the F2000 coating can be confidently described as smooth, while the F100

and F1000 coatings can be characterized as rough surfaces. The surface roughness and the contact angle values decreased as the frequency increased from 100 to 2000 Hz, as shown in Fig. 3. This is attributed to the fact that rougher surfaces (F100) ensnare air bubbles within their pores, inhibiting the formation of hydroxyl bonds between water and the surface, as explained by the Cassie-Baxter model [29].

### 3.2. Phase composition study of coatings

The XRD spectra of the Ti-6Al-4V and all the oxide coatings are illustrated in Fig. 4. In all spectra, the diffraction peaks associated with Ti (ICDD file No. 00-001-1198) were consistently observed, which can be attributed to the porous structure or the thickness of PEO coatings. The distinctive peaks corresponding to the  $\text{ZrTiO}_4$  phase (ICDD file No. 01-080-1783) and rutile phase of  $\text{TiO}_2$  (ICDD file No. 01-082-0514) were also successfully identified. This suggested that  $\text{ZrO}_2$  nanoparticles were subjected to melting due to the high discharge energy. Consequently, these melted nanoparticles reacted with the molten titanium dioxide, resulting in the formation of a new phase (i.e.,  $\text{ZrTiO}_4$ ). Numerous studies [30–33] have reported the reactive incorporation of zirconia particles into the oxide coating that forms on titanium and its alloys. This incorporation has been found to result in the formation of the  $\text{ZrTiO}_4$  (zirconium titanate) phase.

### 3.3. Electrochemical performance of coatings

#### 3.3.1. Potentiodynamic polarization test

Fig. 5 illustrates a potentiodynamic polarization plot in Hank's electrolyte for the substrate and coatings formed at various frequencies. The F100 exhibited different electrochemical behavior compared to F2000 and F1000. As the frequency increased from 100 to 2000 Hz, the potentiodynamic polarization curve shifted towards a more noble potential and a lower corrosion current density. Analysis of the data revealed that coatings produced at 1000 and 2000 Hz exhibited higher corrosion current density compared to the substrate, indicating better corrosion performance compared to the uncoated substrate.

Table 2 presents the electrochemical data obtained from the potentiodynamic polarization curves. The corrosion resistance was calculated using the Stern-Gray equation [34].

$$R_p = \frac{\beta_a \beta_c}{2.3(\beta_a + \beta_c) i_{corr}} \quad (1)$$

Within this equation,  $\beta_a$  and  $\beta_c$  are denoted as the anodic and cathodic slopes, respectively, while  $R_p$  represents the polarization resistance. From the data in Table 2, it's evident that the F2000 sample exhibited the greatest corrosion potential (684 mV), suggesting a relatively lower thermodynamic

tendency for corrosion in comparison to the F1000 and F100 samples. Furthermore, the F2000 sample demonstrated the lowest corrosion current density (13.75 nA/cm<sup>2</sup>) and, as a result, possessed the highest polarization resistance (0.730 M $\Omega$ .cm<sup>2</sup>). By comparing the corrosion resistance of the coat-

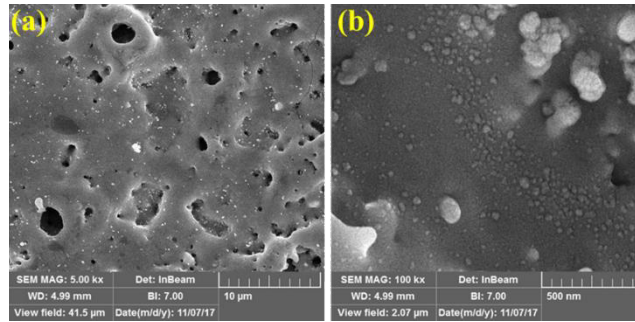


Fig. 2- (a, b) Depict FESEM images of the F2000 sample's surface, captured at varying magnifications.

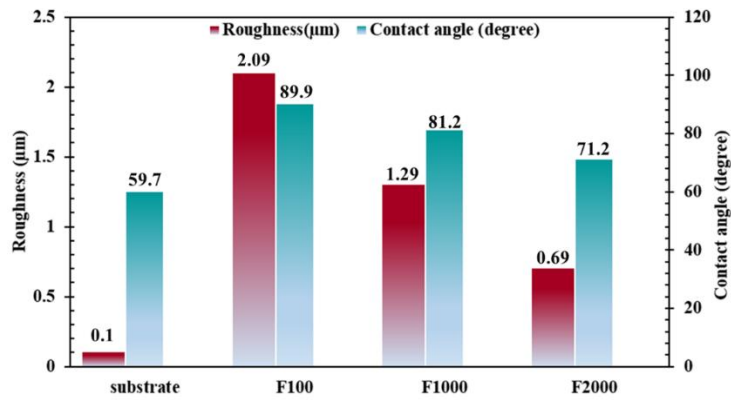


Fig. 3- Relationship between contact angle and roughness.

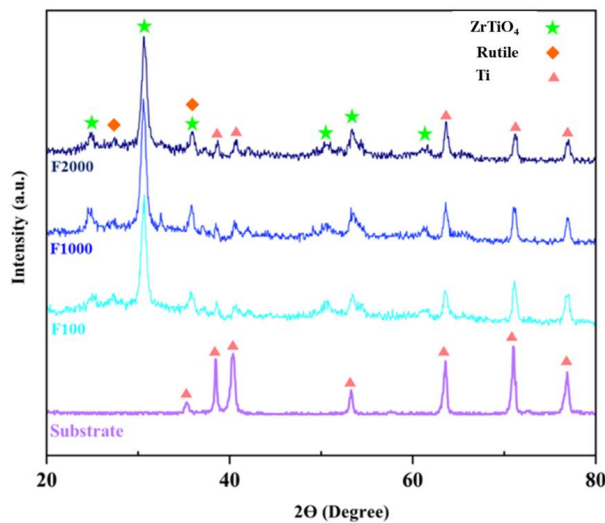


Fig. 4- The XRD patterns of the samples coated at various frequencies.

ings with the reported percentage of porosity, a clear relationship between these two parameters can be observed. As shown earlier, the F2000 and F100 specimens exhibited the lowest and highest porosity percentages, respectively, resulting in the highest and lowest polarization resistance values. Notably, despite having the highest thickness (14.6  $\mu\text{m}$ ), the F100 specimen showed the lowest polarization resistance ( $0.267 \text{ M}\Omega\cdot\text{cm}^2$ ) among all the coatings. This suggested that the thickness of the coating did not have a considerable impact on enhancing the corrosion behavior of the coatings; instead, the porosity percentage of the coatings determined their corrosion properties. This is because corrosive solutions can penetrate into the coating through these porosities, ultimately reaching the substrate and causing damage to the coating. Consequently, the F2000 specimen, with its lower porosity percentage, was better suited to withstand the penetration of corrosive solutions.

**3.3.2. EIS analysis**

Fig. 6 illustrates the EIS plots of the coated specimens and substrate. The Nyquist graphs of coat-

ings in Fig. 6(a) clearly showed the presence of two distinct capacitive loops, indicating a two-layer structure for the coatings [35]. Conversely, the impedance plot of the substrate displayed a single loop, which can be attributed to a formation of a passive film on the surface of the Ti-6Al-4V alloy [36]. Upon comparing the diameters of the curve loops in the Nyquist plot, it becomes evident that the F2000 specimen exhibited the highest semi-circle diameter, indicating the highest level of corrosion resistance. In the bode curves (Fig. 6(b)), it can be observed that at lower frequencies, the impedance values followed the sequence of  $\text{F100} < \text{substrate} < \text{F1000} < \text{F2000}$ . It should also be noted that the impedance values at lower frequencies of F2000, F1000, F100 and substrate were measured to be  $5.7 \times 10^5$ ,  $5.4 \times 10^5$ ,  $5.0 \times 10^5$  and  $5.2 \times 10^5 \Omega\cdot\text{cm}^2$ , respectively. Consequently, the F2000 sample demonstrated the highest impedance value, thus having the most favorable corrosion behavior among all the samples in the Hank's electrolyte.

To simulate the electrochemical performance of both the coatings and the substrate, the equivalent circuits shown in Fig. 7 were utilized. Fig. 7(a)

Table 2- Determined electrochemical properties from PDP plots of coated specimens and substrate

Samples	$R_p$ ( $\text{M}\Omega \text{ cm}^2$ )	$\beta_c$ ( $\text{mV/dec}$ )	$\beta_a$ ( $\text{mV/dec}$ )	$I_{\text{corr}}$ ( $\text{nA/cm}^2$ )	$E_{\text{corr}}$ ( $\text{mV}$ )
Substrate	0.591	78.34	68.23	19.23	-323
F100	0.267	76.84	46.89	47.25	218
F1000	0.602	61.62	44.01	18.50	611
F2000	0.730	69.40	46.89	13.75	684

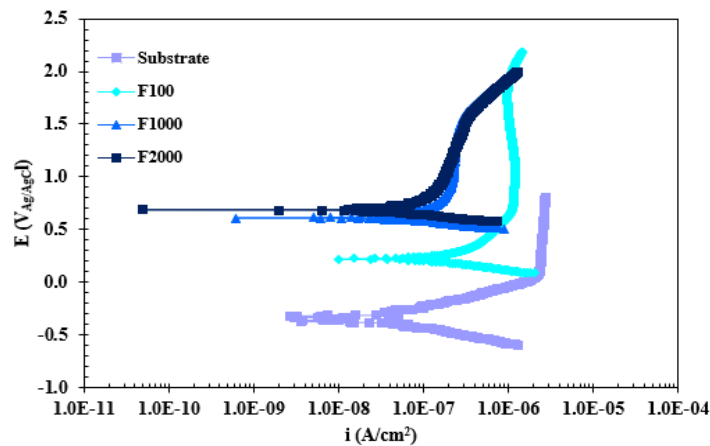


Fig. 5- The PDP plots of coated samples with different frequency.

shows the circuit for the uncoated specimen, where  $R_s$  represents the resistance of the solution, and  $R_i$  and CPE denote the corrosion resistance and constant phase element of the passive film on the Ti-6Al-4V surface, respectively. The coated specimen had the electrical equivalent circuit in Fig. 7(b). Within this circuit, the solution resistance between the surface of the coating and the reference electrode is denoted as  $R_s$ , and the electrical resistance of the inner layer and outer layer are labeled as  $R_i$  and  $R_o$ , respectively. The equivalent circuit employed CPEs in place of ideal resistances due to the heterogeneous nature of the surfaces. The following formula calculates the impedance value of the CPE [37]:

$$Z_{CPE} = \frac{1}{Y_0(jW)^n} \quad (2)$$

In the constant phase element,  $Z_{CPE}$  represents the

impedance,  $W$  denotes the angular frequency, and  $j$  is the square root of  $(-1)$ . The constant phase element is characterized by two key parameters,  $Y_0$  and  $n_0$ .  $Y_0$  corresponds to the admittance, while  $n_0$  is related to the surface roughness. Generally, the value of  $n_0$  can range from 0 to 1. Specifically, the values of 0, 0.5, and 1 correspond to the ideal resistance, Warburg impedance, and ideal capacitor, respectively [16]. Table 3 shows the values of the parameters that were obtained from modeling the electrochemical behavior of the coatings. It is important to note that, irrespective of the varying frequencies of the coatings, the resistance of the solution remained almost unchanged for all three samples, due to the consistent use of the same electrolyte across all experiments. However, the resistance of the inner layer for all the coatings was significantly higher than that of the outer layer, which can be attributed to the presence of fewer defects

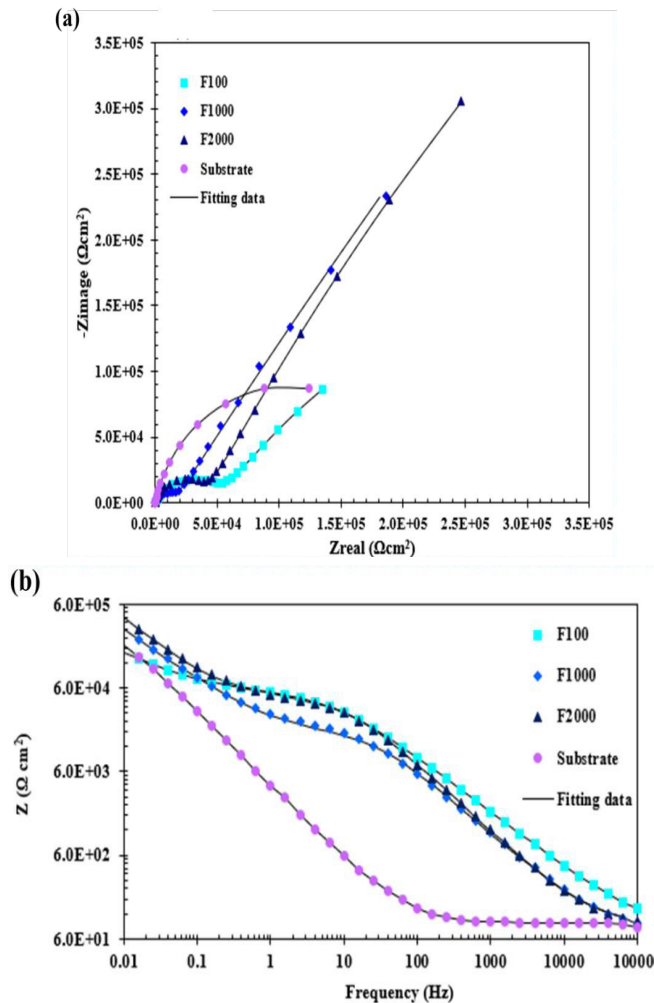


Fig. 6- (a) Nyquist and (b) bode plots of the specimens coated at various frequencies.

and a denser structure. This indicated that the inner layer served as a highly effective barrier against destructive ions due to its lower defect density and compact structure. Furthermore, as the frequency increased from 100 to 2000 Hz, both  $R_i$  and  $R_o$  values also increased. Consequently, the sample produced at 2000 Hz exhibited the highest values of  $R_i$  ( $3.60 \times 10^6 \Omega.cm^2$ ) and  $R_o$  ( $39.28 \times 10^3 \Omega.cm^2$ ). Based on Fig. 6 and contact angle values, it can be inferred that as the frequency level increased, the contact angle decreased (Fig. 3) and the corrosion resistance of coatings improved. According to the findings of Gnedenkov et al. [38], a direct correlation existed between the contact angle and the corrosion resistance of PEO coating. Surprisingly, this study did not observe such a trend. Despite having

the lowest contact angle, the F2000 sample demonstrated the highest corrosion resistance against the corrosive solution. This superior corrosion behavior can be attributed to the lowest percentage of porosity and surface roughness among all the specimens. Indeed, a surface with more roughness could result in an expanded surface area, which could potentially lead to a perceived increase in the rate of corrosion [39].

**4. Conclusion**

The purpose of this research was to investigate the effect of the PEO processing frequency on the microstructure, morphology, and corrosion resistance of the ceramic coatings developed on the Ti-6Al-4V using a phosphate-based electrolyte. Additionally, a

Table 3- Derived data from the suggested equivalent circuit

Sample	$R_s$ ( $\Omega.cm^2$ )	$n_o$	$Q_o$ ( $\mu F.cm^2$ )	$R_o$ ( $K\Omega.cm^2$ )	$n_i$	$Q_i$ ( $\times 10^{-6} S^{\ast}.\Omega^{-1}.cm^{-2}$ )	$R_i$ ( $M\Omega.cm^2$ )
Substrate	64.27	-	-	-	0.731	18.86	2.82
F100	66.45	0.692	1.72	16.40	0.601	37.50	0.70
F1000	74.40	0.774	1.24	18.28	0.646	19.80	3.00
F2000	69.48	0.823	0.70	39.28	0.680	16.75	3.60

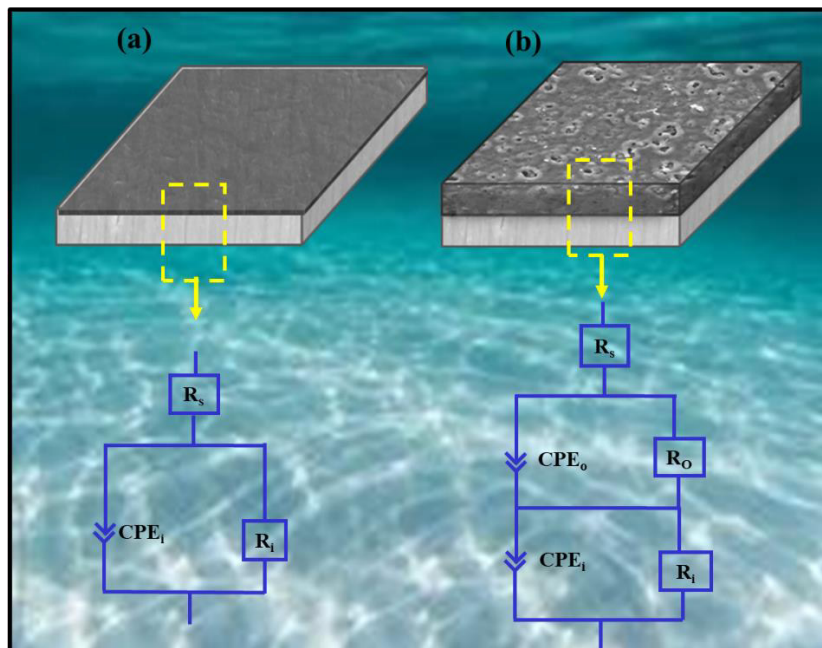


Fig. 7- The equivalent circuit that models the corrosion behavior of (a) substrate and (b) coatings.

comparative examination was carried out between the ceramic coatings and the Ti-6Al-4V substrate, offering valuable insights into the potential advantages and performance improvements offered by PEO-treated surfaces. The results indicated that structural properties of the coatings are notably influenced by the frequency; as the processing frequency increased from 100 to 2000 Hz, there was a noticeable decrease in coating thickness (14.6 to 7.1  $\mu\text{m}$ ), porosity percentage (9.5 to 1.1 %), and average pore diameter (5.8 to 1.7  $\mu\text{m}$ ). Moreover, the

increase in frequency led to a decrease in roughness from 2.1 to 0.7  $\mu\text{m}$  and contact angle from 90° to 71°. The XRD analysis of the coatings indicated that there were no alterations in the phases of the coatings. The potentiodynamic polarization tests revealed that as the frequency escalated from 100 to 2000 Hz, there was a decrease in the corrosion current density and an increase in the corrosion potential. The coating that was formed at 2000 Hz had the lowest corrosion density and the highest corrosion resistance.

## References

- Fattah-alhosseini A, Molaei M. A review of functionalizing plasma electrolytic oxidation (PEO) coatings on titanium substrates with laser surface treatments. *Applied Surface Science Advances*. 2023;18:100506.
- Muhaffel F, Kaba M, Cempura G, Derin B, Kruk A, Atar E, Cimenoglu H. Influence of alumina and zirconia incorporations on the structure and wear resistance of titania-based MAO coatings. *Surface and Coatings Technology*. 2019;377:124900.
- Yerokhin AL, Nie X, Leyland A, Matthews A. Characterisation of oxide films produced by plasma electrolytic oxidation of a Ti-6Al-4V alloy. *Surface and Coatings Technology*. 2000;130(2-3):195-206.
- Roknian M, Fattah-alhosseini A, Gashti SO. Plasma Electrolytic Oxidation Coatings on Pure Ti Substrate: Effects of  $\text{Na}_3\text{PO}_4$  Concentration on Morphology and Corrosion Behavior of Coatings in Ringer's Physiological Solution. *Journal of Materials Engineering and Performance*. 2018;27(3):1343-51.
- Wang J-H, Wang J, Lu Y, Du M-H, Han F-Z. Effects of single pulse energy on the properties of ceramic coating prepared by micro-arc oxidation on Ti alloy. *Applied Surface Science*. 2015;324:405-13.
- Nikoomanzari E, Karbasi M, C.M.A. Melo W, Moris H, Babaei K, Giannakis S, Fattah-alhosseini A. Impressive strides in antibacterial performance amelioration of Ti-based implants via plasma electrolytic oxidation (PEO): A review of the recent advancements. *Chemical Engineering Journal*. 2022;441:136003.
- Attarzadeh N, Kazemi A, Molaei M, Fattah-alhosseini A. Multipurpose surface modification of PEO coatings using tricalcium phosphate addition to improve the bedding for apatite compounds. *Journal of Alloys and Compounds*. 2021;877:160275.
- Aliofkhaezrai M, Macdonald DD, Matykina E, Parfenov EV, Egorkin VS, Curran JA, et al. Review of plasma electrolytic oxidation of titanium substrates: Mechanism, properties, applications and limitations. *Applied Surface Science Advances*. 2021;5:100121.
- Wheeler JM, Collier CA, Paillard JM, Curran JA. Evaluation of micromechanical behaviour of plasma electrolytic oxidation (PEO) coatings on Ti-6Al-4V. *Surface and Coatings Technology*. 2010;204(21-22):3399-409.
- Fattah-Alhosseini A, Keshavarz MK, Molaei M, Gashti SO. Plasma Electrolytic Oxidation (PEO) Process on Commercially Pure Ti Surface: Effects of Electrolyte on the Microstructure and Corrosion Behavior of Coatings. *Metallurgical and Materials Transactions A*. 2018;49(10):4966-79.
- Shokouhfar M, Dehghanian C, Montazeri M, Baradaran A. Preparation of ceramic coating on Ti substrate by plasma electrolytic oxidation in different electrolytes and evaluation of its corrosion resistance: Part II. *Applied Surface Science*. 2012;258(7):2416-23.
- Li G, Ma F, Liu P, Qi S, Li W, Zhang K, Chen X. Review of micro-arc oxidation of titanium alloys: Mechanism, properties and applications. *Journal of Alloys and Compounds*. 2023;948:169773.
- Lu X, Mohedano M, Blawert C, Matykina E, Arrabal R, Kainer KU, Zheludkevich ML. Plasma electrolytic oxidation coatings with particle additions – A review. *Surface and Coatings Technology*. 2016;307:1165-82.
- Fattah-alhosseini A, Molaei M, Babaei K. The effects of nano- and micro-particles on properties of plasma electrolytic oxidation (PEO) coatings applied on titanium substrates: A review. *Surfaces and Interfaces*. 2020;21:100659.
- Fattah-alhosseini A, Chaharmahali R, Babaei K. Impressive strides in amelioration of corrosion and wear behaviors of Mg alloys using applied polymer coatings on PEO porous coatings: A review. *Journal of Magnesium and Alloys*. 2022;10(5):1171-90.
- Nikoomanzari E, Fattah-alhosseini A, Pajohi Alamoti MR, Keshavarz MK. Effect of  $\text{ZrO}_2$  nanoparticles addition to PEO coatings on Ti-6Al-4V substrate: Microstructural analysis, corrosion behavior and antibacterial effect of coatings in Hank's physiological solution. *Ceramics International*. 2020;46(9):13114-24.
- Montazeri M, Dehghanian C, Shokouhfar M, Baradaran A. Investigation of the voltage and time effects on the formation of hydroxyapatite-containing titania prepared by plasma electrolytic oxidation on Ti-6Al-4V alloy and its corrosion behavior. *Applied Surface Science*. 2011;257(16):7268-75.
- Xia Q, Wang J, Liu G, Wei H, Li D, Yao Z, Jiang Z. Effects of electric parameters on structure and thermal control property of PEO ceramic coatings on Ti alloys. *Surface and Coatings Technology*. 2016;307:1284-90.
- Pavarini M, Moscatelli M, Candiani G, Tarsini P, Cochis A, Rimondini L, et al. Influence of frequency and duty cycle on the properties of antibacterial borate-based PEO coatings on titanium for bone-contact applications. *Applied Surface Science*. 2021;567:150811.
- Zhang X, Zhang Y, Chang L, Jiang Z, Yao Z, Liu X. Effects of frequency on growth process of plasma electrolytic oxidation coating. *Materials Chemistry and Physics*. 2012;132(2-3):909-15.
- Karbasi M, Nikoomanzari E, Hosseini R, Bahramian H, Chaharmahali R, Giannakis S, et al. A review on plasma electrolytic oxidation coatings for organic pollutant degradation: How to prepare them and what to expect of them? *Journal of Environmental Chemical Engineering*. 2023;11(3):110027.
- Yerokhin AL, Nie X, Leyland A, Matthews A, Dowey SJ. Plasma electrolysis for surface engineering. *Surface and Coatings Technology*. 1999;122(2-3):73-93.
- Matykina E, Berkani A, Skeldon P, Thompson GE. Real-time

- imaging of coating growth during plasma electrolytic oxidation of titanium. *Electrochimica Acta*. 2007;53(4):1987-94.
24. Aliofkhaezai M, Gharabagh RS, Teimouri M, Ahmadzadeh M, Darband GB, Hasannejad H. Ceria embedded nanocomposite coating fabricated by plasma electrolytic oxidation on titanium. *Journal of Alloys and Compounds*. 2016;685:376-83.
  25. Yao Z, Jiang Z, Sun X, Xin S, Wu Z. Influence of the frequency on the structure and corrosion resistance of ceramic coatings on Ti-6Al-4V alloy produced by micro-plasma oxidation. *Materials Chemistry and Physics*. 2005;92(2-3):408-12.
  26. Bala Srinivasan P, Liang J, Balajee RG, Blawert C, Störmer M, Dietzel W. Effect of pulse frequency on the microstructure, phase composition and corrosion performance of a phosphate-based plasma electrolytic oxidation coated AM50 magnesium alloy. *Applied Surface Science*. 2010;256(12):3928-35.
  27. Lv G-H, Chen H, Gu W-C, Li L, Niu E-W, Zhang X-H, Yang S-Z. Effects of current frequency on the structural characteristics and corrosion property of ceramic coatings formed on magnesium alloy by PEO technology. *Journal of Materials Processing Technology*. 2008;208(1-3):9-13.
  28. Xu L, Wu C, Lei X, Zhang K, Liu C, Ding J, Shi X. Effect of oxidation time on cytocompatibility of ultrafine-grained pure Ti in micro-arc oxidation treatment. *Surface and Coatings Technology*. 2018;342:12-22.
  29. Braem A, Van Mellaert L, Mattheys T, Hofmans D, De Waelheyns E, Geris L, et al. Staphylococcal biofilm growth on smooth and porous titanium coatings for biomedical applications. *Journal of Biomedical Materials Research Part A*. 2013;102(1):215-24.
  30. Molaei M, Fattah-alhosseini A, Nouri M, Mahmoodi P, Navard SH, Nourian A. Enhancing cytocompatibility, antibacterial activity and corrosion resistance of PEO coatings on titanium using incorporated ZrO<sub>2</sub> nanoparticles. *Surfaces and Interfaces*. 2022;30:101967.
  31. Molaei M, Nouri M, Babaei K, Fattah-Alhosseini A. Improving surface features of PEO coatings on titanium and titanium alloys with zirconia particles: A review. *Surfaces and Interfaces*. 2021;22:100888.
  32. Shin KR, Ko YG, Shin DH. Influence of zirconia on biometric apatite formation in pure titanium coated via plasma electrolytic oxidation. *Materials Letters*. 2010;64(24):2714-7.
  33. Gowtham S, Hariprasad S, Arunnellaiappan T, Rameshbabu N. An investigation on ZrO<sub>2</sub> nano-particle incorporation, surface properties and electrochemical corrosion behaviour of PEO coating formed on Cp-Ti. *Surface and Coatings Technology*. 2017 Mar 15;313:263-73.
  34. Lv G-H, Chen H, Li L, Niu E-W, Pang H, Zou B, Yang S-Z. Investigation of plasma electrolytic oxidation process on AZ91D magnesium alloy. *Current Applied Physics*. 2009;9(1):126-30.
  35. Molaei M, Fattah-alhosseini A, Nouri M, Mahmoodi P, Nourian A. Incorporating TiO<sub>2</sub> nanoparticles to enhance corrosion resistance, cytocompatibility, and antibacterial properties of PEO ceramic coatings on titanium. *Ceramics International*. 2022;48(14):21005-24.
  36. Mahlobo MGR, Chikosha L, Olubambi PA. Study of the corrosion properties of powder rolled Ti-6Al-4V alloy applied in the biomedical implants. *Journal of Materials Research and Technology*. 2022;18:3631-9.
  37. Babaei M, Dehghanian C, Babaei M. Electrochemical assessment of characteristics and corrosion behavior of Zr-containing coatings formed on titanium by plasma electrolytic oxidation. *Surface and Coatings Technology*. 2015;279:79-91.
  38. Gnednikov SV, Sinebryukhov SL, Egorkin VS, Mashtalyar DV, Alpysbaeva DA, Boinovich LB. Wetting and electrochemical properties of hydrophobic and superhydrophobic coatings on titanium. *Colloids and Surfaces A: Physicochemical and Engineering Aspects*. 2011;383(1-3):61-6.
  39. Evgeny B, Hughes T, Eskin D. Effect of surface roughness on corrosion behaviour of low carbon steel in inhibited 4 M hydrochloric acid under laminar and turbulent flow conditions. *Corrosion Science*. 2016;103:196-205.